Title

Physical Drivers of Phytoplankton Bloom Initiation in the Southern Ocean's Scotia Sea

Journal

Journal of Geophysical Research: Oceans, 124(8)

ISSN

2169-9275

Authors

Prend, Channing J
Gille, Sarah T
Talley, Lynne D
et al.

Publication Date

2019-08-01

DOI

10.1029/2019jc015162

Peer reviewed

JGR Oceans

RESEARCH ARTICLE
10.1029/2019JC015162

Physical Drivers of Phytoplankton Bloom Initiation in the Southern Ocean's Scotia Sea

Channing J. Prend[1], Sarah T. Gille[1], Lynne D. Talley[1], B. Greg Mitchell[1], Isabella Rosso[1], and Matthew R. Mazloff[1]

[1]Scripps Institution of Oceanography, La Jolla, CA, USA

Key Points:
- Shallow mixed layers in the Scotia Sea support the earliest and largest offshore spring phytoplankton bloom in the Southern Ocean
- About 10% of the water in the bloom region is advected from the Weddell Sea, which helps set the unique stratification
- Vertical transport associated with a stratified Taylor column may enhance productivity by supplying subsurface iron to the euphotic zone

Supporting Information:
- Supporting Information S1

Correspondence to:
C. J. Prend,
cprend@ucsd.edu

Citation:
Prend, C. J., Gille, S. T., Talley, L. D., Mitchell, B. G., Rosso, I., & Mazloff, M. R. (2019). Physical drivers of phytoplankton bloom initiation in the Southern Ocean's Scotia Sea. *Journal of Geophysical Research: Oceans*, *124*. https://doi.org/10.1029/2019JC015162

Received 20 MAR 2019
Accepted 28 JUL 2019
Accepted article online 4 AUG 2019

Abstract The Scotia Sea is the site of one of the largest spring phytoplankton blooms in the Southern Ocean. Past studies suggest that shelf-iron inputs are responsible for the high productivity in this region, but the physical mechanisms that initiate and sustain the bloom are not well understood. Analysis of profiling float data from 2002 to 2017 shows that the Scotia Sea has an unusually shallow mixed-layer depth during the transition from winter to spring, allowing the region to support a bloom earlier in the season than elsewhere in the Antarctic Circumpolar Current. We compare these results to the mixed-layer depth in the 1/6° data-assimilating Southern Ocean State Estimate and then use the model output to assess the physical balances governing mixed-layer variability in the region. Results indicate the importance of lateral advection of Weddell Sea surface waters in setting the stratification. A Lagrangian particle release experiment run backward in time suggests that Weddell outflow constitutes 10% of the waters in the upper 200 m of the water column in the bloom region. This dense Weddell water subducts below the surface waters in the Scotia Sea, establishing a sharp subsurface density contrast that cannot be overcome by wintertime convection. Profiling float trajectories are consistent with the formation of Taylor columns over the region's complex bathymetry, which may also contribute to the unique stratification. Furthermore, biogeochemical measurements from 2016 and 2017 bloom events suggest that vertical exchange associated with this Taylor column enhances productivity by delivering nutrients to the euphotic zone.

Plain Language Summary Tiny algae called phytoplankton form the base of the marine food web and absorb carbon dioxide from the atmosphere through photosynthesis. Therefore, understanding the processes that control the location and timing of phytoplankton blooms is necessary to accurately model marine ecosystems and the global carbon cycle. In this study, we examine the upper ocean conditions that support the earliest and largest offshore spring phytoplankton bloom in the Southern Ocean, which surrounds Antarctica and is a key region of carbon uptake for the global ocean. Observational data and model output both suggest that the bloom region has unique stratification, which is conducive to bloom development. By releasing virtual particles into a climate model and tracking their position, we find that currents transport cold water to the bloom site from the Weddell Sea. This cold water is key to explaining the region's unusual stratification. Finally, we analyze new observations taken by robotic floats of the 2016 and 2017 blooms. These data suggest that biological productivity is closely linked to the seafloor topography. This is because flow over topography leads to enhanced mixing, which delivers essential nutrients to the sunlit upper ocean where phytoplankton can grow.

1. Introduction

The Southern Ocean is typically classified as a high-nutrient low-chlorophyll environment, with phytoplankton growth limited by iron and light (de Baar et al., 1995; Mitchell et al., 1991). The major sources of iron to the Southern Ocean, including shelf sediments, dust deposition, and glacial ice, are highly spatially variable (Lancelot et al., 2009; Tagliabue et al., 2014). Satellite data and in situ measurements show that primary productivity in the Antarctic Circumpolar Current (ACC) is also heterogeneous (Arrigo et al., 2008; Sokolov & Rintoul, 2007; Sullivan et al., 1993). Offshore blooms in the Scotia Sea, far north of the sea ice edge, are sustained for the full austral summer and support nearly half the total circumpolar stock of Antarctic krill (Atkinson et al., 2004; Tarling et al., 2012). Blooms here are triggered particularly early in the season (August–September) compared to other open ocean blooms in the ACC (Holm-Hansen et al., 2004; Murphy et al., 2004), and peak by October–November, when blooms in other parts of the ACC are just being initiated (Blain et al., 2007; Mongin et al., 2008). This is evident in the October satellite chlorophyll

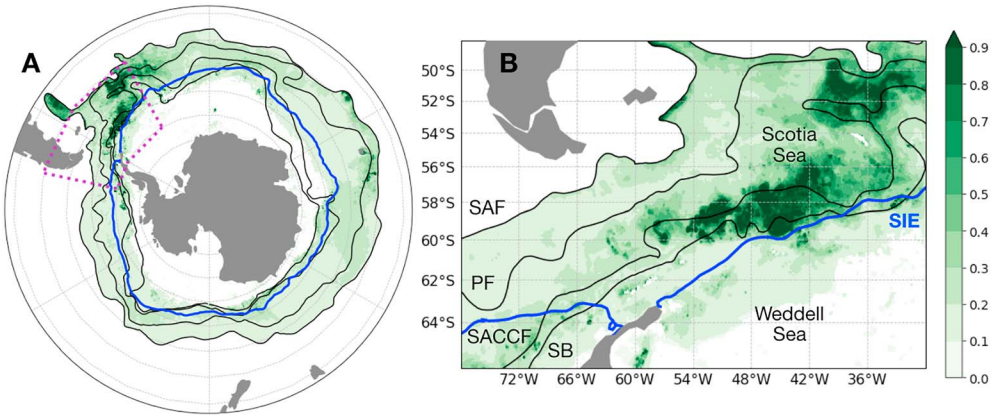

Figure 1. MODIS Aqua satellite 2002–2017 October surface chlorophyll composite (mg/m^3) with major ACC fronts (SAF = Subantarctic Front, PF = Polar Front, SACCF = Southern ACC Front, SB = ACC Southern Boundary) from Orsi et al. (1995) in black and 2002–2017 October Sea Ice Edge (SIE) from NOAA/NSIDC Climate Data Record in blue for (a) the entire Southern Ocean and (b) zoomed in on the Weddell-Scotia region, marked by a magenta box in (a). Note that the SIE is retreating at this time, so the mean position of the SIE during the month of October can overlap with the chlorophyll climatology, which includes data from the full month.

climatology (Figure 1), which shows high chlorophyll in the Scotia Sea (outlined in magenta) while the rest of the Southern Ocean remains low. Therefore, the mechanisms driving bloom initiation in the Scotia Sea have implications for the distribution of Antarctic megafauna as well as carbon export to the ocean interior via the biological pump (Hofmann et al., 1998; Murphy et al., 2004; Murphy et al., 2007).

There are two distinct blooms in the Scotia Sea visible in Figure 1b, a northern bloom located between the Polar Front (PF) and the Southern ACC Front (SACCF) around 51°S and a southern bloom located between the SACCF and the ACC Southern Boundary (SB) around 59°S. The northern bloom has been linked to iron inputs from the South Georgia Islands (Atkinson et al., 2001; Ward et al., 2002). The southern bloom, which is the focus of this study, has different dynamics since it is not associated with an island wake. Instead, iron fluxes from the Antarctic Peninsula have been suggested to support the high productivity in this region (de Jong et al., 2012; Dulaiova et al., 2009; Frants et al., 2013; Hatta et al., 2013). A detailed iron budget of the southern Scotia Sea from a regional coupled physical-biogeochemical model shows that shelf-derived iron can meet most of the demand by the phytoplankton in the region, with minimal contributions from dust, icebergs, and other sources (Jiang et al., 2019). The off-shelf transport of iron-rich waters to the bloom region primarily occurs below the mixed layer and involves multiple processes related to the ACC frontal jets (Frants et al., 2013; Measures et al., 2013; Zhou et al., 2013). For example, horizontal advection and entrainment of shelf waters by the SB were both found to influence iron concentrations in southern Drake Passage (Frants et al., 2013; Measures et al., 2013; Zhou et al., 2013). Further downstream in the Weddell-Scotia confluence, cross-frontal eddy activity at the SACCF was shown to transport nutrients that support phytoplankton growth (Kahru et al., 2007).

The advective pathways hypothesized to deliver iron to the southern Scotia Sea have been examined explicitly using surface drifters (Thompson & Youngs, 2013; Youngs et al., 2015) and particle release experiments in a coupled sea ice-ocean model (Renner et al., 2012). Results support the connection between high Scotia Sea productivity and water properties off the eastern Antarctic Peninsula. These studies have identified how iron, which supports phytoplankton growth through the full austral summer, is transported from the shelf to the bloom region. However, the mechanisms of bloom initiation are still not well understood. Classical theory, known as the critical depth hypothesis, explains spring blooms through shoaling of the mixed layer above a critical depth where vertically integrated phytoplankton growth and losses are equal (Sverdrup, 1953). More recently, Sverdrup's critical depth hypothesis has been questioned for several reasons including its failure to distinguish between the hydrographically defined mixed layer and the actively turbulent layer (Behrenfeld, 2010; Carranza et al., 2018; Franks, 2015; Taylor & Ferrari, 2011). Still, despite the limitations of the critical depth hypothesis, mixed-layer depth (MLD) has been shown to be closely linked to primary

productivity in the Southern Ocean (Carvalho et al., 2017; Fragoso & Smith, 2012; Mitchell et al., 1991; Mitchell & Holm-Hansen, 1991).

In this study, we use float profiles and the eddy-permitting Southern Ocean State Estimate (SOSE) to assess the importance of MLD and other physical factors in initiating and sustaining the southern Scotia Sea bloom. We consider both the climatological hydrographic properties that allow the region to consistently support an early spring bloom as well as the processes that trigger individual bloom events and supply shelf-sourced iron to the euphotic zone. First, we show that year-round shallow mixed layers in the Scotia Sea provide unique conditions conducive to early spring bloom formation. Then we demonstrate the importance of Weddell-Scotia surface exchange in setting this stratification. Finally, we examine spring bloom events in 2016 and 2017 using biogeochemical float data, which allow us to relate changes in bio-optical properties directly to their physical drivers. These observations suggest that strong currents impinging on a seamount in the bloom region support the formation of Taylor columns, which are vertical rotating cylinders of fluid that form when a flow encounters an obstacle (Taylor, 1923). The anticyclonic circulation, counterclockwise in the Southern Hemisphere, and vertical mixing associated with this flow feature are suggested to enhance productivity by providing phytoplankton access to subsurface iron that is advected from the Antarctic Peninsula.

2. Data and Methods

2.1. Profiling Float Data

This study uses hydrographic profiles from floats deployed by both the Argo and the Southern Ocean Carbon and Climate Observations and Modeling (SOCCOM) programs. Argo is a global array currently consisting of more than 3,900 autonomous floats that collect temperature and salinity profiles over the top 2,000 m of the water column every 10 days. These data are made freely available by the International Argo Program and the national programs that contribute to it (http://www.argo.ucsd.edu, http://argo.jcommops.org). We analyze 15,615 profiles collected in the Scotia Sea and surrounding area (48–66°S, 30–76°W) from 2002 to 2017 (Figure 3). The delayed-mode quality-controlled data are used and profiles are interpolated onto a regular depth axis with 5-m vertical resolution. Profiles are binned into different geographic regions based on the mean location of the ACC fronts (Figure 3a). Zonal boundaries of the grid boxes are defined by mean dynamic height contours corresponding to the Subantarctic Front (SAF), PF, and SACCF from Swart et al. (2008). Constant, evenly spaced meridional boundaries were selected in order to fully contain the chlorophyll peak associated with the bloom in the red starred box. The number of profiles in each grid box by month is shown in Figure 3b. The analysis was repeated with several grids in order to test the sensitivity of the results. We varied the longitudinal boundaries of the boxes and the definition of the ACC frontal positions, using isolines of mean dynamic topography based on Sokolov and Rintoul (2009). The analysis was also conducted using a grid of rectangular boxes defined by latitude and longitude only; however, we present results where the grid is based on the ACC fronts as this makes more dynamical sense given the importance of frontal jets in mediating the regional transport.

For each profile, the mixed-layer depth is calculated based on the density criterion following de Boyer Montegut et al. (2004) and using a threshold value of $\Delta\sigma_\theta = 0.03$ kg/m^3 (Dong et al., 2008). Buoyancy frequency (N^2), a measure of the stratification, is found from the density profiles using the Gibbs seawater package routine (http://www.teos-10.org), which has been validated extensively (e.g., King et al., 2012). This routine calculates N^2 from the difference in potential density between two seawater parcels, $\Delta\rho^\Theta$, separated by a small vertical distance Δz, with the reference pressure taken as the midpoint between the two parcels. This is expressed as

$$N^2 = -\frac{g\Delta\rho^\Theta}{\rho\,\Delta z}, \tag{1}$$

where g is the gravitational acceleration and ρ is the density evaluated at the midpressure level. As discussed in King et al. (2012), salinity measurement noise dominates over noise in temperature when calculating buoyancy frequency from CTD data, which can lead to wiggly N^2 profiles. Therefore, N^2 profiles are smoothed using a 10-m vertical running average as in Graff and Behrenfeld (2018).

SOCCOM is a regional array comprising about 125 autonomous Argo-equivalent floats in the Southern Ocean. In addition to collecting temperature and salinity profiles over the top 2,000 m of the water column, the floats also measure dissolved oxygen, nitrate, pH, fluorescence, and backscatter. The data are made freely available by the SOCCOM Project (http://soccom.princeton.edu). The quality-controlled data from the 7 June 2018 SOCCOM snapshot are used in this analysis (http://doi.org/10.17882/42182#58015). In section 3.3 we consider chlorophyll *a* (Chl *a*) profiles calculated from fluorescence for two floats that passed through the southern Scotia Sea during early spring in 2016 and 2017, respectively. Data processing and corrections applied to the Chl *a* fluorometer raw data are described in Johnson et al. (2017). In order to assess the physical factors responsible for triggering bloom events, we compute MLD and euphotic zone depth (Z_e). As for the Argo floats, MLD is calculated using a density threshold of 0.03 kg/m^3. The floats do not directly measure irradiance, so Z_e is calculated from the normalized relationship between euphotic zone depth and chlorophyll column inventory as defined in Morel and Maritorena (2001):

$$\begin{aligned} Z_e &= 912.5\ [\mathrm{Chl_{tot}}]^{-0.839} \quad 10\ \mathrm{m} < Z_e < 102\ \mathrm{m}, \\ Z_e &= 426.3\ [\mathrm{Chl_{tot}}]^{-0.547} \quad 102\ \mathrm{m} < Z_e < 180\ \mathrm{m}, \end{aligned} \tag{2}$$

where $[\mathrm{Chl_{tot}}]$ is the total Chl *a* concentration vertically integrated over the float profile, which is related to the euphotic zone depth by two possible cases depending on the calculated value of Z_e.

2.2. Additional Data

The study also makes use of the 2002–2017 Moderate-Resolution Imaging Spectroradiometer (MODIS) Aqua monthly chlorophyll and photosynthetically available radiation climatologies as well as eight-day MODIS Chl *a* data from spring 2016 and 2017 (http://oceandata.sci.gsfc.nasa.gov/MODIS-Aqua/). For both the monthly and the eight-day fields, the level 3 binned data at 9-km resolution are used. The AVISO combined mean dynamic topography product for 1993–2012 on a 1/4° × 1/4° grid (http://www.aviso.altimetry.fr/) is used to define the mean ACC frontal positions following Swart et al. (2008) and Sokolov and Rintoul (2009). These fronts are used to define a grid for binning float data as described in section 2.1. We note that there is considerable temporal variability in frontal positions, and sea surface height undergoes an annual cycle associated with steric heating and cooling of the ocean. However, our results suggest shallow spring MLDs in the southern Scotia Sea regardless of how the grid is defined, and thus, mean frontal positions are used for simplicity. This is further discussed in section 3.1. NOAA/NSIDC Climate Data Record of monthly passive microwave sea ice concentration is used to plot the sea ice edge (version 3 on a 25 × 25-km grid; https://nsidc.org/data/G02202). Bathymetry from the ETOPO1 1 arc-minute global relief model (Amante & Eakins, 2009) is plotted in several figures and is available online (https://www.ngdc.noaa.gov/mgg/global/). November 2016 surface drifter trajectories from the Global Drifter Program (http://www.aoml.noaa.gov/phod/gdp/index.php) are used to investigate downstream advection of chlorophyll in section 3.3. To this end, we also examine the 1/4° × 1/4° drifter-derived monthly climatology of global near-surface currents (Laurindo et al., 2017). Version 3.03 is used, which is based on data from February 1979 up to July 2018 (http://www.aoml.noaa.gov/phod/gdp/mean_velocity.php).

2.3. Southern Ocean State Estimate

SOSE is an eddy-permitting, data assimilative model that uses ocean observations to constrain the MITgcm solution (Mazloff et al., 2010). The configuration used in this analysis has 1/6° horizontal resolution, 42 uneven vertical levels, and runs from 1 January 2005 to 31 December 2010. A full description of the observational constraints is provided in Mazloff et al. (2010), which includes shipboard CTD measurements, Argo float profiles, and instrument-mounted elephant seal profiles. This iteration of the model has been extensively validated (Abernathey et al., 2016; Cerovečki et al., 2011; Cerovečki & Mazloff, 2015) and is publicly available (http://sose.ucsd.edu). In section 3.1, SOSE state variables are used to calculate buoyancy frequency and MLD. In section 3.2, the bloom region heat and salt budgets are computed from SOSE output to examine the drivers of mixed-layer variability. SOSE diagnoses heat and salt budget terms at each grid point from the model state and outputs them as five-day averages. The heat budget is computed following Tamsitt et al. (2016), where the temperature evolution is given by the sum of the air-sea heat flux, advective heat transport (separated into geostrophic and ageostrophic components), and three-dimensional diffusive processes:

$$\underbrace{\frac{\partial T}{\partial t}}_{\text{temperature tendency}} = \underbrace{\frac{Q(z)}{\rho c_p dz}}_{\text{air-sea flux}} - \underbrace{\mathrm{u}_g \cdot \nabla T}_{\text{geostrophic advection}} - \underbrace{\mathrm{u}_a \cdot \nabla T}_{\text{ageostrophic advection}} + \underbrace{\kappa_H \nabla_H^2 T + \kappa_z \frac{\partial^2 T}{\partial z^2} + K_T^{turb}}_{\text{diffusion}}, \quad (3)$$

where $\partial T/\partial t$ is the temperature tendency, Q is the net air-sea heat flux, c_p is the specific heat capacity of seawater, dz is the depth in the model over which Q is distributed, $\mathbf{u}_g$ and $\mathbf{u}_a$ are the geostrophic and ageostrophic horizontal velocities, ∇ is the divergence operator, κ_H and κ_z are the horizontal and vertical diffusivities, and K_T^{turb} is the K-profile parameterization turbulent vertical diffusion term (Large et al., 1994). As in Tamsitt et al. (2016), geostrophic velocities are calculated from the model hydrostatic pressure, and ageostrophic velocities are taken to be the residual between the model velocity and calculated geostrophic velocity.

The salt budget can be expressed in a similar way, as described by Cerovečki et al. (2019). The key difference from the heat budget is the surface flux term, which is determined by the net effects of evaporation, precipitation, runoff, and freshwater forcing by sea ice processes. The full salt budget is

$$\underbrace{\frac{\partial S}{\partial t}}_{\text{salinity tendency}} = \underbrace{\frac{S}{dz}(\mathrm{E}-\mathrm{P}-\mathrm{R}-\mathrm{IO})}_{\text{surface freshwater flux}} - \underbrace{\mathrm{u}_g \cdot \nabla S}_{\text{geostrophic advection}} - \underbrace{\mathrm{u}_a \cdot \nabla S}_{\text{ageostrophic advection}} + \underbrace{\kappa_H \nabla_H^2 S + \kappa_z \frac{\partial^2 S}{\partial z^2} + K_S^{turb}}_{\text{diffusion}}, \quad (4)$$

where $\partial S/\partial t$ is the salinity tendency, E is the evaporation, P is the precipitation, R is the runoff, and IO is the freshwater forcing by sea ice processes. Advection and diffusion terms are defined as in the heat budget but computed using the divergence of salinity rather than temperature.

Also, SOSE daily velocity fields are used to calculate off-line Lagrangian particle trajectories using the particle-tracking model Octopus, which is available online (http://github.com/jinbow/Octopus). Details of the interpolation scheme have been described by van Sebille et al. (2018) and by Tamsitt et al. (2017, 2018). For the purposes of this study, we seed particles in the southern Scotia Sea and then run trajectories backward in time by using reversed velocities. This is done in order to determine the bloom region source waters and their relative fractions. In particular, particles were released at three SOSE vertical levels (150, 177.5, and 208.5 m) in a rectangular box (evenly spaced horizontally) enclosing the bloom site with boundaries 57.5°–59°S, 43°–47°W (outlined in black in Figure 5). This depth range was chosen as it is below the average MLD in the region and roughly the depth at which shelf-sourced iron is advected to the Scotia Sea (150–200 m; Frants et al., 2013). Particles were run backward in time for a period of nine months, which was found to be the approximate time necessary for the Lagrangian particles to be advected from the Weddell Sea to the bloom region. In total, 120,000 particles were released in 12 separate runs beginning on the first day of every month in 2010. The runs were partitioned in order to use SOSE velocity fields from different nine-month periods in an attempt to account for any seasonal variability that may impact particle pathways.

3. Results

3.1. Regional Mixed-Layer Variability

A unique aspect of the southern Scotia Sea bloom is how early in the season it occurs compared to other open ocean blooms in the ACC. Here, bloom events are typically triggered in mid-August to September and peak by November (Hewes et al., 2008; Murphy et al., 2004), whereas blooms in other parts of the ACC are triggered in late October to November (Blain et al., 2007; Mongin et al., 2008). To investigate why bloom initiation is so early in the Scotia Sea, we first examine the physical conditions in the region during early spring. A useful diagnostic to consider is the buoyancy frequency, N^2, which is a measure of the water column stability. Higher N^2 values indicate stronger stratification, which inhibits vertical mixing of the phytoplankton and thus aids biomass accumulation necessary to bloom development (Brody & Lozier, 2015). The map in Figure 2a shows the SOSE subsurface N^2 maximum during the early austral spring period, defined as 15 August to 15 September (composite of all years in the SOSE run). This is compared to Figure 2b, which gives the subsurface N^2 maximum calculated at individual Argo profiles from 15 August to 15 September during

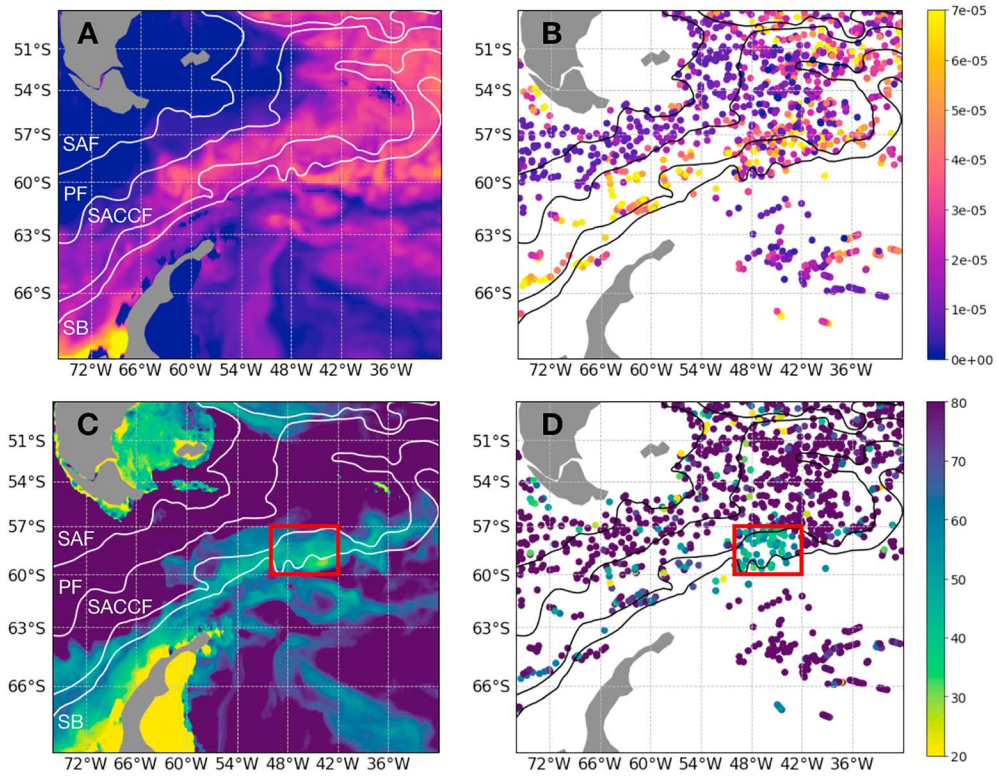

Figure 2. Subsurface N^2 maximum (s^{-2}) (a) in SOSE and (b) at individual Argo profiles during the early spring period (15 August–15 September). Also, the depth in the water column (m) where this maximum occurred, roughly the base of the mixed layer (c) in SOSE and (d) from Argo. The red box in (c) and (d) highlights shallower than average MLD in the bloom region. Orsi et al. (1995) fronts plotted, as in Figure 1.

the SOSE period (2005–2010). The overall spatial pattern of buoyancy frequency is consistent between SOSE and Argo, with higher N^2 values between the PF and SACCF. Note though that 2005–2010 Argo data are assimilated into SOSE. While it may not be particularly surprising then that SOSE shows similar patterns in MLD, it is necessary to establish this fact in order to justify the usefulness of using SOSE to assess the mixed-layer heat and salt budgets in the following section of the paper. Overall, the bloom region has a relatively high buoyancy frequency, signifying a more stably stratified water column that is favorable to bloom development. However, the values are comparable to other locations along the SACCF.

The bloom region is more distinctive when we consider the depth in the water column where the subsurface N^2 maximum occurs, which has been shown to be an ecologically relevant depth corresponding to phytoplankton vertical distribution (Carvalho et al., 2017). This is plotted for SOSE in Figure 2c and for individual Argo profiles in Figure 2d. Based on the definition of the buoyancy frequency (equation (1)), this is the depth with the maximum vertical density gradient, which is similar to the hydrographically defined MLD in many cases. In general, Figures 2c and 2d show that smaller values of N^2 correspond to deeper N^2 maxima. Compared to other locations, the N^2 maxima in the bloom region occur at shallower depths in the water column. This is particularly apparent in Figure 2d if one considers the patch of shallower maximum N^2 depth values between 42°W and 50°W south of the SACCF (red boxes in Figures 2c and 2d), which corresponds to shallower MLD as well. Overall, the spatial distribution of MLD is similar in structure to Figures 2c and 2d (see Figure S2 in the supporting information). In other words, the southern Scotia Sea seems to have a shallower MLD than nearby regions during the bloom initiation period. This is consistent with the classical explanation for spring phytoplankton blooms, which suggests that shallow mixed layers facilitate rapid bloom development by providing phytoplankton with more access to light and nutrients (Sverdrup, 1953).

To further characterize regional MLD, we bin Argo profiles from the Scotia Sea and surrounding area (48–66°S, 30–76°W) into a grid based on the mean location of the ACC frontal positions and compute a monthly climatology of MLD for all 12 boxes. This is shown in Figure 3c based on Argo profiles (top

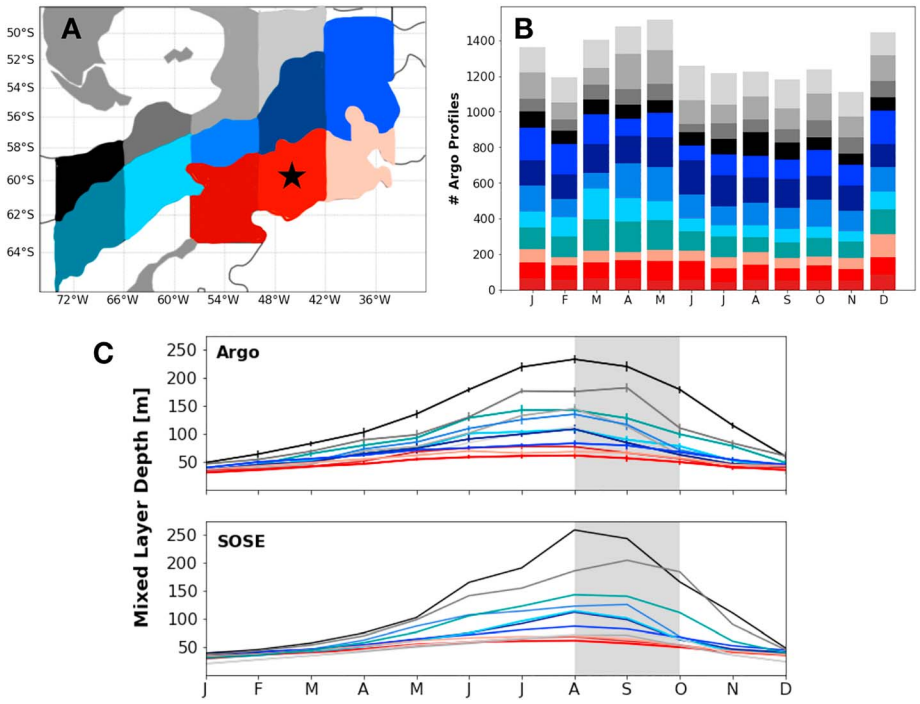

Figure 3. (a) Map showing the grid for Argo analysis based on frontal positions defined by mean dynamic topography contours from Swart et al. (2008). A black star marks the box containing the bloom site. (b) Histogram showing the number of Argo profiles located within each grid box by month. In total 15,615 profiles from 2002 to 2017 were used. (c) Monthly averaged mixed layer depth (m) for each grid box in (a) from Argo profiles (top panel) with error bars marking the 95% confidence interval and SOSE (bottom panel). Gray shading highlights August and September, the typical bloom initiation months.

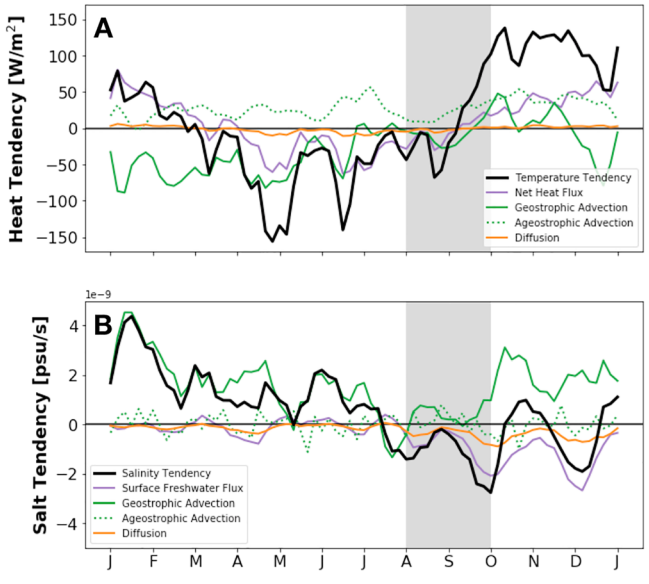

Figure 4. The 2005–2010 mean SOSE (a) heat budget (positive values signify heating) and (b) salt budget (positive values signify salinification) spatially averaged over the bloom region (red starred box in Figure 2a) and vertically integrated over the top 53 m (SOSE vertical level closest to the average mixed-layer depth). Gray shading highlights August and September, the typical bloom initiation months.

panel) as well as SOSE (bottom panel). Both Argo and SOSE show that the red starred box (bloom region) has a markedly shallow MLD during the bloom initiation period of August and September (highlighted in gray in Figure 3c). This stratification allows the southern Scotia Sea to support phytoplankton growth earlier in the season, since a bloom can occur as soon as spring light levels increase. Results consistently showed shallow MLD in the bloom region, regardless of the choice of grid (not shown). However, the seasonal cycle in the bloom region is not statistically different at the 95% confidence level from the other two regions south of the SACCF (different shades of red in Figure 3a). Therefore, MLD alone cannot explain why the bloom occurs at this particular location. Furthermore, how are nutrients supplied to the euphotic zone in the absence of wintertime MLD deepening? These questions are investigated after first examining why the regions south of the SACCF have a shallow year-round MLD.

3.2. Weddell-Scotia Surface Exchange

Comparatively shallow MLDs in the southern Scotia Sea allow the region to support an early spring bloom. Here we assess the physical balances that govern upper ocean variability in the region. Figure 4 shows the 2005–2010 mean SOSE heat and salt budget. The temperature tendency (black in Figure 4a) is driven mainly by surface heat fluxes (purple in Figure 4a) and geostrophic advection (green in Figure 4a). Air-sea heat flux follows the expected seasonal cycle with positive values in summer (i.e., heat entering the ocean) and negative values in winter (heat

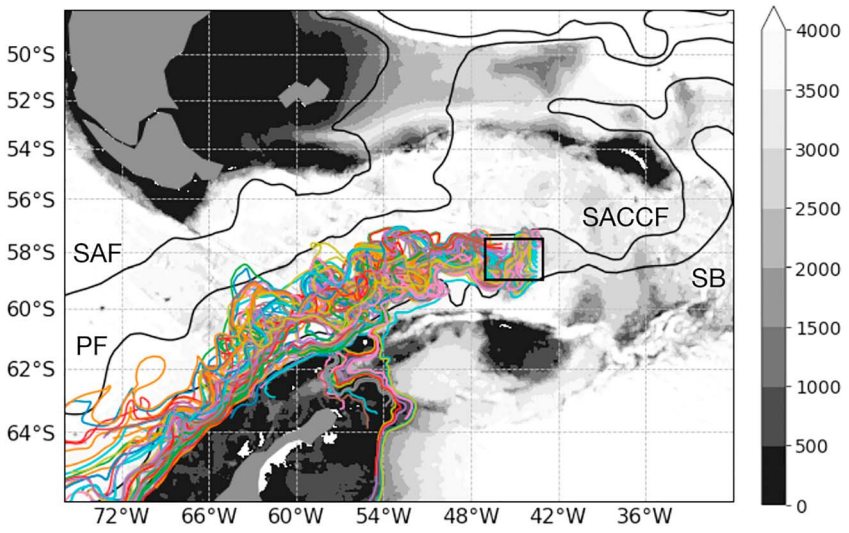

Figure 5. ETOPO1 bathymetry (shading; m) with 100 randomly selected back trajectories from SOSE particle release experiment. Black box marks where particles were seeded. Orsi et al. (1995) fronts plotted in black.

leaving the ocean). Horizontal geostrophic advection acts to cool the mixed layer during most of the year. This is consistent with the transport of cold Weddell water to the Scotia Sea, which has been observed from drifter data (Thompson & Youngs, 2013; Youngs et al., 2015). Geostrophic advection is also an important driver of the salinity tendency (black in Figure 4b). Next, we examine the role of Weddell outflow in setting the bloom region stratification. This influence, for example, could be due to the stratifying effects of freshwater from ice melt. Another possibility is that the Weddell water, which is cold and dense, subducts below the surface waters in the bloom region and creates a stable floor to the base of the mixed layer. These hypotheses are explored through a Lagrangian particle release experiment.

Of the 120,000 particles seeded in the southern Scotia Sea and run backward in time, 100 randomly selected trajectories are plotted in Figure 5. In the forthcoming discussion, "initial position" refers to the particle's location away from the bloom region after being run backward in time for nine months. Similarly, "final position" refers to the location in the bloom region where the particle was seeded. One can see qualitatively that most of the water in the top 200 m of the bloom region comes from the ACC, with a small fraction originating in the Weddell. Based on all the trajectories, this fraction is equal to 10%, which is quantified by finding the number of particles with an initial position east of 57°W. To test the sensitivity of our results, smaller runs were also conducted using velocity fields from nine-month periods in other years of the SOSE run; SOSE spans only six years, so large-scale climate variability is not captured. While precise pathways and rates varied slightly, results regarding the fraction of Weddell-sourced waters in the bloom region were consistent.

Figure 6a shows two particular trajectories that were selected to illustrate the major pathways taken by waters to reach the upper 200 m of the bloom region. The orange trajectory represents the 90% of total particles that originate upstream in the ACC, while the blue trajectory represents the 10% of total particles that are advected from the Weddell Sea. These trajectories are then mapped in θ-S space (Figure 6b). The Weddell particle is colder and saltier at its initial position (marked by a blue triangle) than it is once it reaches the bloom region (blue square). Furthermore, the particle is initially near the surface and then increases its depth along the trajectory (see Figure S3 in the supporting information). On average, Weddell-sourced particles increase their depth by 104 m while traveling to the bloom region. This supports the hypothesis that Weddell water subducts below the surface waters in the ACC, stabilizing the mixed layer in the bloom region. The ACC particle on the other hand starts out warmer and lighter (orange triangle) compared to its final position (orange square), and its depth varies much less along the trajectory (standard deviation of 11 m).

To demonstrate that these two particles are representative of the two source waters to the bloom region, we use θ and salinity from the initial positions of all trajectories to calculate a joint probability density function

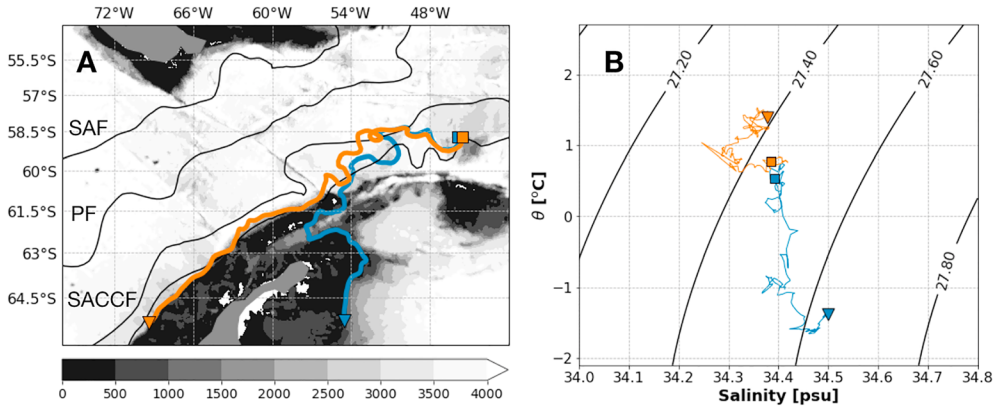

Figure 6. (a) ETOPO1 bathymetry (shading; m) with two modeled particle trajectories representative of the major pathways traveled by waters that reach the bloom region. Orsi et al. (1995) fronts plotted in black. (b) The θ-S properties along the trajectories in (a).

(Figure 7). A red square marks the average θ-S properties of particles at their final location in the Scotia Sea. Figure 7 shows two distinct source waters: a broadly defined water mass centered close to the initial position of the ACC particle in Figure 6b and a smaller peak near the initial Weddell particle position in Figure 6b. In general, the ACC source water is warmer and lighter than the particle's final θ and salinity (red square), consistent with modification by the 10% of the colder and denser Weddell water.

Given that we have two distinct source waters, along with estimates of their average θ-S properties and relative fractions, it is tempting to add them together in an informal Optimum Multiparameter (OMP) analysis (Tomczak & Large, 1989). OMP is an inverse modeling technique that describes observed water properties at a particular location as a mixture of several different source waters. Following this framework, one could take a weighted sum of the two source waters identified from the joint probability density function. Doing so certainly shifts the ACC source water closer to the bloom region θ and salinity. However, the OMP method assumes that advection moves water along isopycnals, and Figure 6b clearly shows that particle pathways are not strictly adiabatic. While the cold Weddell water likely plays a role in setting the bloom region θ-S properties, some diabatic processes are also necessary along the particle trajectories. This may be due to mixing over the region's rough topography, which has been observed in the Ona Basin, for example (Barré et al., 2008). In the case of the Weddell particles, which are initially near the surface, modification by air-sea fluxes and sea ice processes along the particle pathways is also possible (see supporting information for an estimate of these surface fluxes).

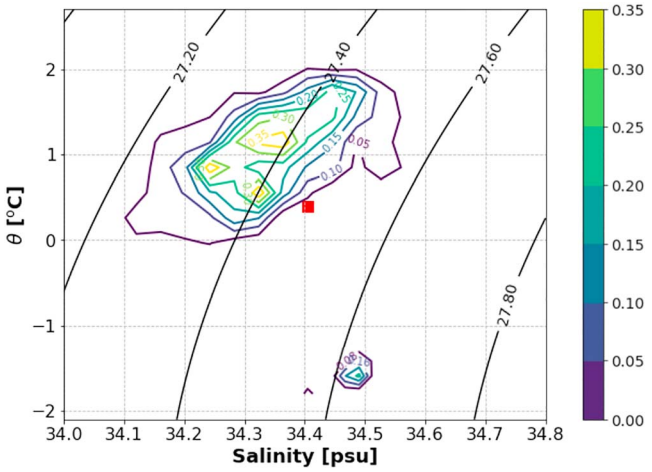

Figure 7. Joint probability density function of modeled particle θ (°C) and salinity (psu) at the particle's initial position after being run backward in time for nine months. Red box marks the average θ-S properties of the modeled particles at their final position in the bloom region.

3.3. Individual Bloom Events

Thus far, we have considered the climatological conditions in the Scotia Sea based on several years of data and SOSE output. In this section we examine 2016 and 2017 bloom events as measured by SOCCOM floats WMO 5904660 and 5904984, respectively. Float 5904660 entered the southern Scotia Sea from the west on 3 September 2016. Starting on 23 September, Chl a increased rapidly before peaking in early November (see Figure 8c). MODIS satellite chlorophyll data from this period confirm that the high Chl a measured by the float was the signature of a large-scale bloom (not shown). The MLD (purple) and Z_e (black) deepen just before the bloom begins. Thus, while the stratification in the Scotia Sea makes the region a good candidate for an early spring bloom, mixed-layer shoaling is not necessarily responsible for triggering individual bloom events. What did trigger the bloom then? Increasing spring light levels, as indicated by Z_e deepening, are likely important. We also note that high chlorophyll corresponds to the five-month period when the float was trapped in

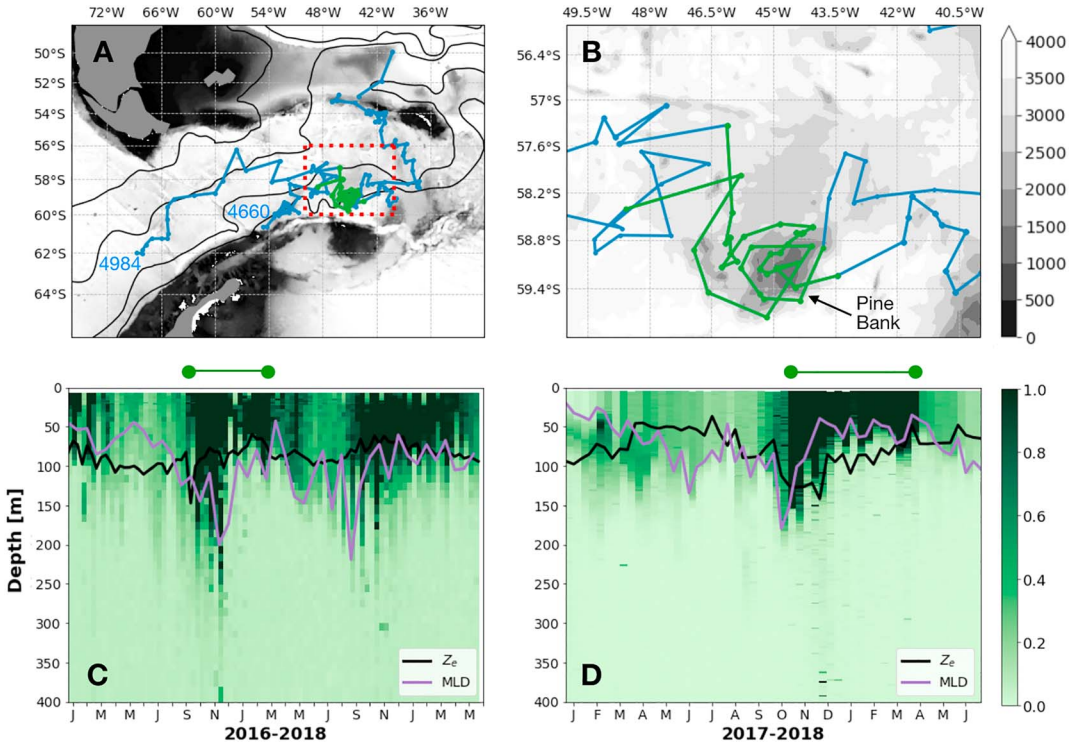

Figure 8. (a) ETOPO1 bathymetry (shading; m) with float 5904660 and 5904984 trajectories and (b) zoomed in on the bloom region and Pine Bank (c) float 5904660 and (d) float 5904984 Chl *a* (mg/m^3) with MLD (purple; m) and Z_e (black; m) overlaid. Green portion of the trajectory corresponds to the period of high float Chl *a* (i.e., bloom period).

an anticyclonic flow over a topographic feature called Pine Bank (Figure 8b). Furthermore, the drop in Chl *a* after 7 March 2017 occurred when the float escaped from the rise.

Similarly, high Chl *a* was measured by float 5904984 when it was trapped in an anticyclonic circulation over Pine Bank during the 2017–2018 bloom cycle (Figure 8d). The abrupt drop in Chl *a* after 25 March 2018 coincided with the float's escape from the seamount. This indicates that the bathymetry and associated circulation may have important biological implications. In addition to the SOCCOM floats discussed here, examination of the Argo database yields seven other floats from 2005 to 2016 that circled on top of Pine Bank for several months, suggesting that this is a frequent flow feature. Furthermore, the November satellite chlorophyll climatology (Figure 9) shows a plume of high Chl *a* extending away from Pine Bank. The plume is consistent with the pathways suggested by the November drifter-derived climatology of global near-surface currents (white arrows) as well as individual surface drifter trajectories from November 2016 (magenta), when SOCCOM float data recorded high chlorophyll over Pine Bank. This implies that advection may also redistribute the chlorophyll produced at Pine Bank across the wider bloom region.

4. Discussion

Biogeochemical float data from both 2016 and 2017 showed high Chl *a* corresponding to the floats being trapped in an anticyclonic circulation over Pine Bank. Closed loops in Argo trajectories over seamounts may indicate the presence of Taylor columns (Meredith et al., 2015). Furthermore, Meredith et al. (2015) mapped the locations most likely to form Taylor columns within the Southern Ocean using regional bathymetry with SOSE velocity fields and stratification. The Scotia Sea, including this particular bank, was among the locations identified. Results of Meredith et al. (2015) are based on a simple dimensional analysis described by Huppert (1975). We follow this calculation here to confirm that Taylor columns can occur over Pine Bank. Taylor column formation requires rotational terms in the equations of motion to dominate, so we first compute the Burger number, $B = NH/fL$, which compares stratification and rotation, where N is the Brunt-Väisälä frequency, H is the local depth away from the bathymetric feature, f is the Coriolis

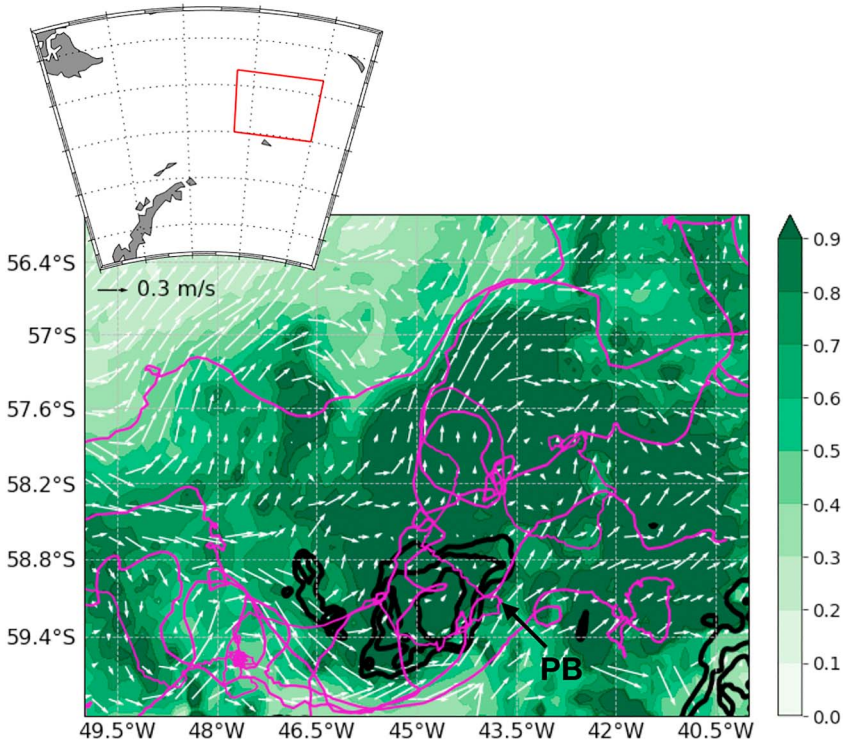

Figure 9. MODIS Aqua satellite 2002–2017 November surface chlorophyll composite (mg/m^3) for Pine Bank (PB) region, with black contours outlining ETOPO1 bathymetry shallower than 3,000 m (500-m intervals). White arrows denote the November drifter-derived climatology of global near-surface currents. Individual surface drifter trajectories from November 2016 are also shown (magenta).

parameter, and L is the horizontal length scale of the feature. Using approximate values $N \approx 5.5 \times 10^{-3}$ s (computed as the average from the 2002–2017 bloom region Argo data), $H \approx 3{,}500$ m, $f = 1.25 \times 10^{-4}$ s, and $L \approx 150$ km, yields $B \approx 1$. Then, we calculate the Rossby number, $Ro = U/fL$, which compares the inertial and rotation terms in the equation of motion, where U is the horizontal velocity scale. For $U \approx 0.2$ m/s (from SOSE velocity fields), and f and L given above, $Ro \approx 0.01$. Finally, we can compute the critical height (h_0/Ro) from the scaled height of the bathymetric feature $h_0 = h/H$, where h is the height of the rise. With $h \approx 1{,}700$ m and H given above, $h_0 \approx 0.49$, which gives a critical height of $h_0/Ro \approx 49$. This value is an order of magnitude larger than the critical value of ~1.3–2 found by Huppert (1975), see their Figure 3, for $B \approx 1$). This indicates that the geometry of Pine Bank favors Taylor column formation, and confirms the results from Meredith et al. (2015).

The role of Taylor columns in enhancing productivity has been recognized at other locations including Cobb seamount in the North Pacific (Dower et al., 1992) and the Prince Edward Plateau in the Indian sector of the Southern Ocean (Perissinotto & Duncombe Rae, 1990). These studies proposed several mechanisms for how Taylor columns impact biological production including buildup of nutrients due to recirculation and retention of local waters, and increased stability of the surface mixed layer. Both of these processes may be at play in the southern Scotia Sea. Isopycnals often dome in a Taylor column, causing shoaling of the mixed-layer base as was observed at Bruce and Discovery Banks (downstream of Pine Bank) by Meredith et al. (2015). Iron delivery to the euphotic zone via vertical exchanges is also likely important. The off-shelf transport of iron to the Scotia Sea occurs primarily on the $\sigma_\theta = 27.5$ isopycnal (Frants et al., 2013). At the bloom site, downstream of the shelf iron source, the depth of this iron-enriched isopycnal is about 150–200 m during September in SOSE. This may explain why the blooms in 2016 and 2017 were triggered immediately following a deepening of the MLD since phytoplankton would have been able to access the subsurface iron. However, past studies suggest that light limitation is likely more significant than iron limitation for phytoplankton in early spring (Mitchell et al., 1991). Furthermore, MLD varies on time scales shorter than the full

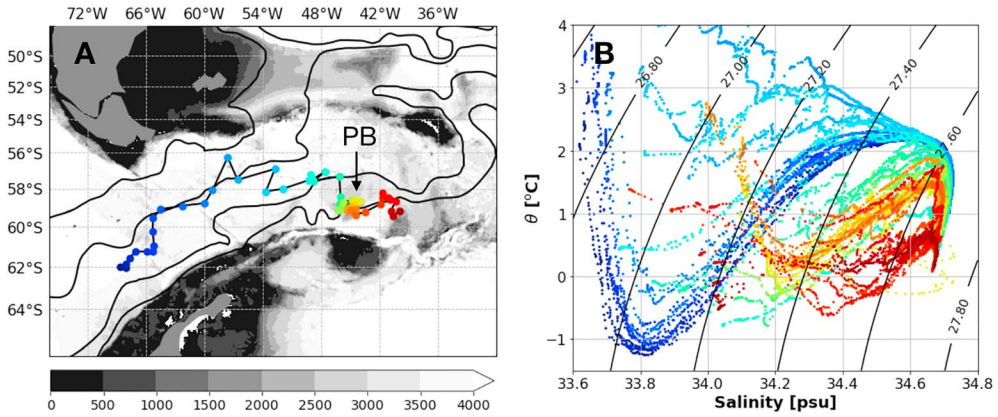

Figure 10. (a) ETOPO1 bathymetry (shading; m) with SOCCOM float 5904984 trajectory, stations where the float took profiles are colored progressively from blue to red. Pine Bank (PB) is marked by an arrow and Orsi et al. (1995) fronts plotted in black. (b) Float θ-S properties colored by the corresponding stations along the trajectory in (a).

bloom cycle, so vertical fluxes of iron across the base of the mixed layer are necessary to sustain the bloom beyond its initial stage.

While the classical Taylor column regime is not associated with vertical velocities, Sévellec et al. (2015) showed theoretically and from moored observations in northern Drake Passage that vertical transports can occur in a stratified Taylor column. This vertical transport compensates for changes in horizontal flow orientation with depth due to stratification (Sévellec et al., 2015). Indeed, SOCCOM profiles of Chl a, temperature, salinity, and oxygen all indicate vigorous vertical mixing when floats 5904660 and 5904984 came over Pine Bank. This is illustrated by the θ-S diagram of float 5904984 (Figure 10). At the point where the float reaches Pine Bank (transition from blues to greens in Figure 10), θ-S properties undergo a complete change in character. Temperature, for example, loses both the freezing surface water and the warmest temperature maximum. We should note that this also corresponds to the crossing of ACC streamlines, and floats may not be sampling the same water mass in progressive profiles. Still, recirculation over Pine Bank retains and mixes waters in the region for months at a time, suggesting that Taylor columns are important to local water mass modification. Furthermore, the recirculation may assist in the transfer of biomass to higher trophic levels, helping explain the region's unusually high abundance of krill, whales, and other megafauna (Atkinson et al., 2004; Hofmann et al., 1998; Murphy et al., 2004; Murphy et al., 2007).

In addition to Taylor column effects, the observed mixing over Pine Bank could be related to other flow-topography interactions. For example, diapycnal mixing is typically higher over topographic features due to breaking internal tides, as well as scattering and breaking of remotely generated internal waves (Kunze et al., 2006; Polzin et al., 1997; Whalen et al., 2012). Submesoscale instabilities in the lee of topography have also been shown to enhance vertical exchange (Rosso et al., 2014; Rosso et al., 2015). Observation-based estimates of the diffusivity in the Scotia Sea (e.g., Balwada et al., 2016; Naveira Garabato et al., 2004) show mixing rates over rough topography that are 2 to 3 orders of magnitudes greater than background values. Furthermore, these high diffusivities extend far above the topography and were shown by Mashayek et al. (2017) to lead to the fast vertical spreading of tracers in a high-resolution ocean model of the Drake Passage region. Another possible explanation for the vertical transports over Pine Bank is upwelling due to Ekman divergence associated with the anticyclonic circulation. Namely, divergence could occur because the northern part of Pine Bank, where winds and surface currents oppose each other, has stronger wind stress; while the southern part of Pine Bank, where winds and currents are aligned, has lower wind stress. In order to better characterize the vertical mixing and its role in driving primary production, a dedicated field campaign including biogeochemical and microstructure measurements would be informative.

5. Conclusion

The highly productive southern Scotia Sea bloom system has been the subject of investigation for decades (Hofmann et al., 1998; Holm-Hansen et al., 2004; Kahru et al., 2007; Murphy et al., 2004), yet the

mechanisms initiating and sustaining the bloom are not well understood. Using Argo data and SOSE, we show that the climatological mixed layer in the region is markedly shallow (<70 m) year-round, which supports early spring bloom formation. We then use SOSE to investigate the processes that set this stratification. Mixed-layer heat and salt budgets indicate the importance of horizontal advection. A backward (in time) particle release experiment is then conducted to determine the source waters that constitute the top 200 m of the water column in the bloom region. We find that 90% of the water comes from upstream in the ACC, while the remaining 10% originates in the Weddell Sea. The Scotia Sea water cannot be defined explicitly as a weighted sum of these two source waters since the particles originating in the Weddell are initially near the surface and therefore subject to significant change through air-sea interaction and sea ice freshwater fluxes. Still, the Weddell outflow is cold and dense enough that it likely modifies the ACC water and contributes to the unique stratification in the bloom region.

While this stratification makes the region prone to early spring bloom development, mixed-layer depth alone cannot explain why the bloom occurs at this particular location since the MLD seasonal cycle in the bloom region is not statistically different from the other regions south of the SACCF. The year-round shallow MLD also raises the question of how nutrients are supplied to the euphotic zone in the absence of winter mixed-layer deepening. Biogeochemical profiling float data suggest that topographic mixing processes are key in determining the bloom location and delivering nutrients to the surface ocean. The highest Chl *a* levels were measured by floats trapped in an anticyclonic circulation over a topographic feature called Pine Bank. Closed loops in float trajectories over seamounts have been shown to indicate the presence of Taylor columns. This is consistent with the results of Meredith et al. (2015), who found that the Scotia Sea, with its complex bathymetry, is one of the regions most likely to form Taylor columns in the Southern Ocean. Biological impacts of Taylor columns in other locations have been noted in past studies (Dower et al., 1992; Meredith et al., 2003; Perissinotto & Duncombe Rae, 1990). However, this is the first observational evidence of this mechanism in relation to the southern Scotia Sea bloom.

From the limited available data, we cannot unequivocally confirm the existence of a Taylor column or determine if Taylor column formation is necessary to bloom development in this region. Regardless, there is a strong connection between the topography and chlorophyll levels. We propose that the bloom is triggered by increasing spring light levels and then sustained past its initial stages by vertical transports associated with a stratified Taylor column that continue to supply iron to the base of the mixed layer. Isopycnal doming in the Taylor column and restratification processes associated with Weddell-Scotia surface exchange also likely contribute to bloom development at Pine Bank, as well as proximity to an upstream shelf iron source. Furthermore, satellite chlorophyll data suggest that this localized process affects the wider Scotia Sea bloom region through downstream advection. Therefore, other regions within the Southern Ocean identified by Meredith et al. (2015) as favorable to Taylor column formation (e.g., Kerguelen Plateau, Maud Rise) deserve further examination to assess the role that this circulation plays in driving primary production.

Acknowledgments
C.J.P. is supported by a National Science Foundation Graduate Research Fellowship under grant DGE-1650112. S.T.G., L.D.T., I.R., and M.R.M. were supported by NSF PLR-1425989. S.T.G. also received support from NSF OCE-1658001. B.G.M. was supported by NSF ANT-0948338. The authors thank two anonymous reviewers, whose comments greatly improved the manuscript. Thanks also to Emma Bent for helping get Octopus running and Ivana Cerovečki for assisting with the SOSE budgets. Profiling float data were collected and made freely available the International Argo Program (http://www.argo.ucsd.edu, http://argo.jcommops.org) and by the Southern Ocean Carbon and Climate Observations and Modeling (SOCCOM) Project (http://soccom.princeton.edu) funded by the National Science Foundation, Division of Polar Programs (NSF PLR-1425989), supplemented by NASA (NNX14AP49B), and by Argo and the NOAA programs that contribute to it. Southern Ocean State Estimate (SOSE) output is publicly available (http://sose.ucsd.edu). Offline Lagrangian particle trajectories were calculated using Octopus (http://github.com/jinbow/Octopus). AVISO combined mean dynamic topography product for 1993–2012 on a 1/4° × 1/4° grid is available online (http://www.aviso.altimetry.fr/). MODIS Aqua level 3 binned chlorophyll *a* data at 9-km resolution are available from NASA (http://oceandata.sci.gsfc.nasa.gov/MODIS-Aqua/). Bathymetry from the ETOPO1 Global Relief Model is available from NOAA (https://www.ngdc.noaa.gov/mgg/global/). Surface drifter trajectories are available from the Global Drifter Program (http://www.aoml.noaa.gov/phod/gdp/index.php). The drifter-derived monthly climatology of global near-surface currents on a 1/4° × 1/4° is also available from NOAA (http://www.aoml.noaa.gov/phod/gdp/mean_velocity.php). NOAA/NSIDC Climate Data Record of passive microwave sea ice concentration is available online (https://nsidc.org/data/G02202).

References

Abernathey, R. P., Cerovečki, I., Holland, P. R., Newsom, E., Mazloff, M. R., & Talley, L. D. (2016). Water-mass transformation by sea ice in the upper branch of the Southern Ocean overturning. *Nature Geoscience*, *9*(8), 596–601. https://doi.org/10.1038/ngeo2749

Amante, C., & Eakins, B. W. (2009). ETOPO1 1 arc-minute global relief model: Procedures, data sources, and analysis. NOAA Technical Memorandum NESDIS NGDC-24. National Geophysical Data Center, NOAA.

Arrigo, K. R., van Dijken, G. L., & Bushinsky, S. (2008). Primary production in the Southern Ocean, 1997–2006. *Journal of Geophysical Research*, *113*, C08004. https://doi.org/10.1029/2007JC004551

Atkinson, A., Siegel, V., Pakhomov, E., & Rothery, P. (2004). Long-term decline in krill stock and increase in salps within the Southern Ocean. *Nature*, *432*(7013), 100–103. https://doi.org/10.1038/nature02996

Atkinson, A., Whitehouse, M. J., Priddle, J., Cripps, G. C., Ward, P., & Brandon, M. A. (2001). South Georgia, Antarctica: A productive, cold water, pelagic ecosystem. *Marine Ecology Progress Series*, *216*, 279–308. https://doi.org/10.3354/meps216279

Balwada, D., Speer, K. G., LaCasce, J. H., Owens, W. B., Marshall, J., & Ferrari, R. (2016). Circulation and stirring in the southeast Pacific Ocean and the Scotia Sea sectors of the Antarctic Circumpolar Current. *Journal of Physical Oceanography*, *46*(7), 2005–2027. https://doi.org/10.1175/JPO-D-15-0207.1

Barré, N., Provost, C., Sennechael, N., & Lee, J. H. (2008). Circulation in the Ona Basin, southern Drake Passage. *Journal of Geophysical Research*, *113*, C04033. https://doi.org/10.1029/2007JC004549

Behrenfeld, M. J. (2010). Abandoning Sverdrup's critical depth hypothesis on phytoplankton blooms. *Ecology*, *91*(4), 977–989. https://doi.org/10.1890/09-1207.1

Blain, S., Queguiner, B., Armand, L., Belviso, S., Bombled, B., Bopp, L., et al. (2007). Effect of natural iron fertilization on carbon sequestration in the Southern Ocean. *Nature*, *446*(7139), 1070–1074. https://doi.org/10.1038/nature05700

Brody, S. R., & Lozier, M. S. (2015). Characterizing upper-ocean mixing and its effect on the spring phytoplankton bloom with *in situ* data. *ICES Journal of Marine Science*, *72*(6), 1961–1970. https://doi.org/10.1093/icesjms/fsv006

Carranza, M. M., Gille, S. T., Franks, P. J. S., Johnson, K. S., Pinkel, R., & Girton, J. B. (2018). When mixed layers are not mixed. Storm-driven mixing and bio-optical vertical gradients in mixed layers of the Southern Ocean. *Journal of Geophysical Research: Oceans*, *123*, 7264–7289. https://doi.org/10.1029/2018JC014416

Carvalho, F., Kohut, J., Oliver, M. J., & Schofield, O. (2017). Defining the ecologically relevant mixed-layer depth for Antarctica's coastal seas. *Geophysical Research Letters*, *44*, 338–345. https://doi.org/10.1002/2016GL071205

Cerovečki, I., & Mazloff, M. R. (2015). The spatiotemporal structure of diabatic processes governing the evolution of Subantarctic Mode Water in the Southern Ocean. *Journal of Physical Oceanography*, *46*, 683–710.

Cerovečki, I., Meijers, A. J., Mazloff, M. R., Gille, S. T., Tamsitt, V. M., & Holland, P. R. (2019). The effects of enhanced sea ice export from the Ross Sea on recent cooling and freshening of the Southeast Pacific. *Journal of Climate*, *32*, 2013–2035. https://doi.org/10.11175/JCLI-D-18-0205.1

Cerovečki, I., Talley, L. D., & Mazloff, M. R. (2011). A comparison of Southern Ocean air-sea buoyancy flux from an ocean state estimate with five other products. *Journal of Climate*, *24*(24), 6283–6306. https://doi.org/10.1175/2011JCLI3858.1

de Baar, H. J. W., de Jong, J., Baaker, D., Loscher, B. M., Veth, C., Bathmann, U., & Smetacek, V. (1995). Importance of iron for plankton blooms and carbon dioxide drawdown in the Southern Ocean. *Nature*, *373*(6513), 412–415. https://doi.org/10.1038/373412a0

de Boyer Montegut, C., Madec, G., Fischer, S., Lazar, A., & Iudicone, D. (2004). Mixed layer depth over the global ocean: An examinatino of profile data and a profile-based climatology. *Journal of Geophycial Research*, *109*, C12003. https://doi.org/10.1029/2004JC002378

de Jong, J., Schoemann, V., Lannuzel, D., Croot, P., de Barr, H., & Tison, J.-L. (2012). Natural iron fertilization of the Atlantic sector of the Southern Ocean by continental shelf sources of the Antarctic Peninsula. *Journal of Geophysical Research*, *117*, G01029. https://doi.org/10.1029/2011JG001679

Dong, S., Sprintall, J., Gille, S. T., & Talley, L. D. (2008). Southern Ocean mixed-layer depth from Argo float profiles. *Journal of Geophysical Research*, *113*, C06013. https://doi.org/10.1029/2006JC004051

Dower, J., Freeland, H., & Juniper, K. (1992). A strong biological response to oceanic flow past Cobb Seamount. *Deep-Sea Research*, *39*(7-8), 1139–1145. https://doi.org/10.1016/0198-0149(92)90061-W

Dulaiova, H., Ardelan, M. V., Henderson, P. B., & Charette, M. A. (2009). Shelf-derived iron inputs drive biological productivity in the southern Drake Passage. *Global Biogeochemical Cycles*, *23*, GB4014. https://doi.org/10.1029/2008GB003406

Fragoso, G. M., & Smith, W. O. (2012). Influence of hydrography on phytoplankton distribution in the Amundsen and Ross Seas, Antarctica. *Journal of Marine Systems*, *89*(1), 19–29. https://doi.org/10.1016/j.jmarsys.2011.07.008

Franks, P. J. S. (2015). Has Sverdrup's critical depth hypothesis been tested? Mixed layers vs. turbulent layers. *ICES Journal of Marine Science*, *72*(6), 1897–1907. https://doi.org/10.1093/icesjms/fsu175

Frants, M., Gille, S. T., Hatta, M., Hiscock, W. T., Kahru, M., Measures, C. I., et al. (2013). Analysis of horizontal and vertical processes contributing to natural iron supply in the mixed layer in southern Drake Passage. *Deep-Sea Research II*, *90*, 68–76. https://doi.org/10.1016/j.dsr2.2012.06.001

Graff, J. R., & Behrenfeld, M. J. (2018). Photoacclimation responses in subarctic Atlantic phytoplankton following a natural mixing-restratification event. *Frontiers in Marine Science*, *5*, 209. https://doi.org/10.3389/fmars.2018.00209

Hatta, M., Measures, C. I., Selph, K. E., Zhou, M., & Hiscock, W. T. (2013). Iron fluxes from the shelf regions near the South Shetland Islands in the Drake Passage during the austral-winter 2006. *Deep-Sea Research II*, *90*, 89–101. https://doi.org/10.1016/j.dsr2.2012.11.003

Hewes, C. D., Reiss, C. S., Kahru, M., Mitchell, B. G., & Holm-Hansen, O. (2008). Control of phytoplankton biomass by dilution and mixed layer depth in the western Weddell-Scotia Confluence. *Marine Ecology Progress Series*, *366*, 15–29. https://doi.org/10.3354/meps07515

Hofmann, E. E., Klinck, J. M., Locarnini, R. A., Fach, B., & Murphy, E. (1998). Krill transport in the Scotia Sea and environs. *Antarctic Science*, *10*(4), 406–415. https://doi.org/10.1017/S0954102098000492

Holm-Hansen, O., Naganobu, M., Kawaguchi, S., Kameda, T., Krasovski, I., Tchernyshkov, P., et al. (2004). Factors influencing the distribution, biomass, and productivity of phytoplankton in the Scotia Sea and adjoining waters. *Deep-Sea Research II*, *51*(12-13), 1333–1350. https://doi.org/10.1016/j.dsr2.2004.06.015

Huppert, H. E. (1975). Some remarks on the initiation of inertial Taylor columns. *Journal of Fluid Mechanics*, *67*(2), 397–412. https://doi.org/10.1017/S0022112075000377

Jiang, M., Measures, C. I., Barbeau, K. A., Charette, M. A., Gille, S. T., Hatta, M., et al. (2019). Fe sources and transport from the Antarctic Peninsula shelf to the southern Scotia Sea. *Deep-Sea Research I*, 103060. https://doi.org/10.1016/j.dsr.2019.06.006

Johnson, K. S., Plant, J. N., Coletti, L. J., Jannasch, H. W., Sakamoto, C. M., Riser, S. C., et al. (2017). Biogeochemical sensor performance in the SOCCOM profiling float array. *Journal of Geophysical Research: Oceans*, *122*, 6416–6436. https://doi.org/10.1002/2017JC012838

Kahru, M., Mitchell, B. G., Gille, S. T., Hewes, C. D., & Holm-Hansen, O. (2007). Eddies enhance biological production in the Weddell-Scotia confluence of the Southern Ocean. *Geophysical Research Letters*, *34*, L14603. https://doi.org/10.1029/2007GL030430

King, B., Stone, M., Zhang, H. P., Gerkema, T., Marder, M., Scott, R. B., & Swinney, H. L. (2012). Buoyancy frequency profiles and internal semidiurnal tide turning depths in the oceans. *Journal of Geophysical Research*, *117*, C04008. https://doi.org/10.1029/2011JC007681

Kunze, E., Firing, E., Hummon, J. M., Chereskin, T. K., & Thurnherr, A. M. (2006). Global abyssal mixing inferred from lowered ADCP shear and CTD strain profiles. *Journal of Physical Oceanography*, *36*(8), 1553–1576. https://doi.org/10.1175/JPO2926.1

Lancelot, C., de Montety, A., Goosse, H., Becquevort, S., Schoemann, V., Pasquer, B., & Vancoppenolle, M. (2009). Spatial distribution of the iron supply to phytoplankton in the Southern Ocean: A model study. *Biogeosciences*, *6*(12), 2861–2878. https://doi.org/10.5194/bg-6-2861-2009

Large, W. G., McWilliams, J. C., & Doney, S. C. (1994). Oceanic vertical mixing: A review and a model with a nonlocal boundary layer parameterization. *Reviews of Geophysics*, *32*(4), 363–403. https://doi.org/10.1029/94RG01872

Laurindo, L., Mariano, A., & Lumpkin, R. (2017). An improved near-surface velocity climatology for the global ocean from drifter observations. *Deep-Sea Research I*, *124*, 73–92. https://doi.org/10.1016/j.dsr.2017.04.009

Mashayek, A., Ferrari, R., Merrifield, S., Ledwell, J. R., St Laurent, L., & Naveira Garabato, A. C. (2017). Topographic enhancement of vertical turbulent mixing in the Southern Ocean. *Nature Communications*, *8*(1), 14,197. https://doi.org/10.1038/ncomms14197

Mazloff, M. R., Heimbach, P., & Wunsch, C. (2010). An eddy permitting Southern Ocean state estimate. *Journal of Physical Oceanography*, *40*(5), 880–899. https://doi.org/10.1175/2009JPO4236.1

Measures, C. I., Brown, M. T., Selph, K. E., Apprill, A., Zhou, M., Hatta, M., & Hiscock, W. T. (2013). The influence of shelf processes in delivering dissolved iron to the HNLC waters of the Drake Passage, Antarctica. *Deep-Sea Research II*, *90*, 77–88. https://doi.org/10.1016/j.dsr2.2012.11.004

Meredith, M. P., Meijers, A. S., Naveira Garabato, A. C., Brown, P. J., Venables, H. J., Abrahamsen, E. P., et al. (2015). Circulation, retention, and mixing of waters within the Weddell-Scotia Confluence, Southern Ocean: The role of stratified Taylor columns. *Journal of Geophysical Research: Oceans*, *120*, 547–562. https://doi.org/10.1002/2014JC010462

Meredith, M. P., Watkins, J. L., Murphy, E. J., Cunningham, N. J., Wood, A. G., Korb, R., et al. (2003). An anticyclonic circulation above the Northwest Georgia Rise, Southern Ocean. *Geophysical Research Letters*, *30*(20), 2061. https://doi.org/10.1029/2003GL018039

Mitchell, B. G., Brody, E. A., Holm-Hansen, O., McClain, C., & Bishop, J. (1991). Light limitation of phytoplankton biomass and macronutrient utilization in the Southern Ocean. *Limnology and Oceanography*, *36*(8), 1662–1677. https://doi.org/10.4319/lo.1991.36.8.1662

Mitchell, B. G., & Holm-Hansen, O. (1991). Observations and modeling of the Antarctic phytoplankton crop in relation to mixing depth. *Deep-Sea Research I*, *38*(8-9), 981–1007. https://doi.org/10.1016/0198-0149(91)90093-U

Mongin, M., Molina, E., & Trull, T. W. (2008). Seasonality and scale of the Kerguelen plateau phytoplankton bloom: A remote sensing and modeling analysis of the influence of natural iron fertilization in the Southern Ocean. *Deep-Sea Research II*, *55*(5-7), 880–892. https://doi.org/10.1016/j.dsr2.2007.12.039

Morel, A., & Maritorena, S. (2001). Bio-optical properties of oceanic waters: A reappraisal. *Journal of Geophysical Research*, *106*(C4), 7163–7180. https://doi.org/10.1029/2000JC000319

Murphy, E. J., Thorpe, S. E., Watkins, J. L., & Hewitt, R. (2004). Modeling the krill transport pathway in the Scotia Sea: Spatial and environmental connections generating the seasonal distribution of krill. *Deep-Sea Research II*, *51*(12-13), 1435–1456. https://doi.org/10.1016/S0967-0645(04)00090-6

Murphy, E. J., Watkins, J. L., Trathan, P. N., Reid, K., Meredith, M. P., Thorpe, S. E., et al. (2007). Spatial and temporal operation of the Scotia Sea ecosystem: A review of large-scale links in a krill centred food web. *Philosophical Transactions of the Royal Society B*, *362*(1477), 113–148. https://doi.org/10.1098/rstb.2006.1957

Naveira Garabato, A. C., Polzin, K. L., King, B. A., Heywood, K. J., & Visbeck, M. (2004). Widespread intense turbulent mixing in the Southern Ocean. *Science*, *303*(5655), 210–213. https://doi.org/10.1126/science.1090929

Orsi, A. H., Whitworth, T. III, & Nowlin, W. D. Jr. (1995). On the meridional extent and fronts of the Antarctic Circumpolar Current. *Deep-Sea Research I*, *42*(5), 641–673. https://doi.org/10.1016/0967-0637(95)00021-W

Perissinotto, R., & Duncombe Rae, C. M. (1990). Occurrence of anticyclonic eddies on the Prince Edward Plateau (Southern Ocean): Effects on phytoplankton biomass and production. *Deep-Sea Research I*, *37*(5), 777–793. https://doi.org/10.1016/0198-0149(90)90006-H

Polzin, K. L., Toole, J. M., Ledwell, J. R., & Schmitt, R. W. (1997). Spatial variability of turbulent mixing in the abyssal ocean. *Science*, *276*(5309), 93–96. https://doi.org/10.1126/science.276.5309.93

Renner, A. H. H., Thorpe, S. E., Heywood, K. J., Murphy, E. J., Watkins, J. L., & Meredith, M. P. (2012). Advective pathways near the tip of the Antarctic Peninsula: Trends, variability and ecosystem implications. *Deep-Sea Research I*, *63*, 91–101. https://doi.org/10.1016/j.dsr.2012.01.009

Rosso, I., Hogg, A. M. C., Kiss, A. E., & Gayen, B. (2015). Topographic influence on submesoscale dynamics in the Southern Ocean. *Geophysical Research Letters*, *42*, 1139–1147. https://doi.org/10.1002/2014GL062720

Rosso, I., Hogg, A. M. C., Strutton, P. G., Kiss, A. E., Matear, R., Klocker, A., & van Sebille, E. (2014). Vertical transport in the ocean due to sub-mesoscale structures: Impacts in the Kerguelen region. *Ocean Modelling*, *80*, 10–23. https://doi.org/10.1016/j.ocemod.2014.05.001

Sévellec, F., Naveira Garabato, A. C., Brearley, J. A., & Sheen, K. L. (2015). Vertical flow in the Southern Ocean estimated from individual moorings. *Journal of Physical Oceanography*, *45*(9), 2209–2220. https://doi.org/10.1175/JPO-D-14-0065.1

Sokolov, S., & Rintoul, S. R. (2007). On the relationship between fronts of the Antarctic Circumpolar Current and surface chlorophyll concentrations in the Southern Ocean. *Journal of Geophysical Research*, *112*, C07030. https://doi.org/10.1029/2006JC004072

Sokolov, S., & Rintoul, S. R. (2009). Circumpolar structure and distribution of the Antarctic Circumpolar Current fronts: 2. Variability and relationship to sea surface height. *Journal of Geophysical Research*, *114*, C11019. https://doi.org/10.1029/2008JC005248

Sullivan, C. W., Arrigo, K. R., McClain, C. R., Comiso, J. C., & Firestone, J. (1993). Distributions of phytoplankton blooms in the Southern Ocean. *Science*, *262*(5141), 1832–1837. https://doi.org/10.1126/science.262.5141.1832

Sverdrup, H. U. (1953). On conditions for the vernal blooming of phytoplankton. *ICES Journal of Marine Science*, *18*(3), 287–295. https://doi.org/10.1093/icesjms/18.3.287

Swart, S., Speich, S., Ansorge, I. J., Goni, G. J., Gladyshev, S., & Lutjeharms, J. R. E. (2008). Transport and variability of the Antarctic Circumpolar Current south of Africa. *Journal of Geophysical Research*, *113*, C09014. https://doi.org/10.1029/2007JC004223

Tagliabue, A., Sallee, J.-B., Bowie, A. R., Levy, M., Swart, S., & Boyd, P. W. (2014). Surface-water iron supplies in the Southern Ocean sustained by deep winter mixing. *Nature Geoscience*, *7*(4), 314–320. https://doi.org/10.1038/ngeo2101

Tamsitt, V., Abernathey, R. P., Mazloff, M. R., Wang, J., & Talley, L. D. (2018). Transformation of deep water masses along Lagrangian upwelling pathways in the Southern Ocean. *Journal of Geophysical Research: Oceans*, *123*, 1994–2017. https://doi.org/10.1002/2017JC013409

Tamsitt, V., Drake, H. F., Morrison, A. K., Talley, L. D., Dufour, C. O., Gray, A. R., et al. (2017). Spiraling pathways of global deep waters to the surface of the Southern Ocean. *Nature Communications*, *8*(1), 172. https://doi.org/10.1038/s41467-017-00197-0

Tamsitt, V., Talley, L. D., Mazloff, M. R., & Cerovečki, I. (2016). Zonal variations in the Southern Ocean heat budget. *Journal of Climate*, *29*(18), 6563–6579. https://doi.org/10.1175/JCLI-D-15-0630.1

Tarling, G. A., Ward, P., Atkinson, A., Collins, M. A., & Murphy, E. (2012). DISCOVERY 2010: Spatial and temporal variability in a dynamic polar ecosystem. *Deep-Sea Research II*, *59*, 1–13.

Taylor, G. I. (1923). Experiments on the motion of solid bodies in rotating fluids. *Proceedings of the Royal Society A*, *106*, 213–218.

Taylor, J. R., & Ferrari, R. (2011). Shutdown of turbulent convection as a new criterion for the onset of spring phytoplankton blooms. *Limnology and Oceanography*, *56*(6), 2293–2307. https://doi.org/10.4319/lo.2011.56.6.2293

Thompson, A. F., & Youngs, M. K. (2013). Surface exchange between the Weddell and Scotia Seas. *Geophysical Research Letters*, *40*, 5920–5925. https://doi.org/10.1002/2013GL058114

Tomczak, M., & Large, D. G. B. (1989). Optimum multiparameter analysis of mixing in the thermocline of the Eastern Indian Ocean. *Journal of Geophysical Research*, *94*(C11), 16,141–16,149. https://doi.org/10.1029/JC094iC11p16141

van Sebille, E., Griffies, S. M., Abernathey, R., Adams, T. P., Berloff, P., Biastoch, A., et al. (2018). Lagrangian ocean analysis: Fundamentals and practices. *Ocean Modelling*, *121*, 49–75. https://doi.org/10.1016/j.ocemod.2017.11.008

Ward, P., Whitehouse, M., Meredith, M., Murphy, E., Shreeve, R., Korb, R., et al. (2002). The southern Antarctic Circumpolar Current front: Physical and biological coupling at South Georgia. *Deep-Sea Research I*, *49*(12), 2183–2202. https://doi.org/10.1016/S0967-0637(02)00119-X

Whalen, C. B., Talley, L. D., & MacKinnon, J. A. (2012). Spatial and temporal variability of global ocean mixing inferred from Argo profiles. *Geophysical Research Letters*, *39*, L18612. https://doi.org/10.1029/2012GL053196

Youngs, M. K., Thompson, A. F., Flexas, M. M., & Heywood, K. J. (2015). Weddell Sea export pathways from surface drifters. *Journal of Physical Oceanography*, *45*(4), 1068–1085. https://doi.org/10.1175/JPO-D-14-0103.1

Zhou, M., Zhu, Y., Measures, C. I., Hatta, M., Charette, M. A., Gille, S. T., et al. (2013). Winter mesoscale circulation on the shelf slope region of the southern Drake Passage. *Deep-Sea Research II*, *90*, 4–14. https://doi.org/10.1016/j.dsr2.2013.03.041